Spectroscopic and Magnetic Properties of $[FeL_2(salacen)]PF_6$ (L = Imidazole or *N*-Methylimidazole): New Examples of Intermediate Electronic Relaxation between $S = \frac{1}{2}$ and $S = \frac{5}{2}$ States. *X*-Ray Crystal Structure of $[Fe(Him)_2(salacen)]PF_6$†

Yonezo Maeda* and Yoshimasa Takashima
Department of Chemistry, Faculty of Science, Kyushu University, Hakozaki, Higashiku, Fukuoka 812, Japan
Naohide Matsumoto and Akira Ohyoshi
Department of Industrial Chemistry, Faculty of Engineering, Kumamoto University, Kurokami 2-39-1, Kumamoto 860, Japan

The iron(III) complexes $[FeL_2(salacen)]PF_6$ [L = imidazole (Him) or *N*-methylimidazole (mim), salacen = ethylene(*N*-acetylacetonylideneiminate)(*N'*-α-methylsalicylideneiminate)] were synthesized, and the phenomenon of the spin transition between high-spin ($S = \frac{5}{2}$) and low-spin ($S = \frac{1}{2}$) states depending on temperature was confirmed by temperature-dependent magnetism and Mössbauer spectra. The time-averaged Mössbauer spectra between the high-spin and low-spin states were observed for $[Fe(mim)_2(salacen)]PF_6$. A stochastic model was proposed to estimate a spin-interconversion rate from the Mössbauer spectra of spin-crossover complexes. The spin-interconversion rates of 6.7×10^6 s^{-1} at 298 K and 3.1×10^6 s^{-1} at 221 K were estimated using the model. Crystals of $[Fe(Him)_2(salacen)]PF_6$ are triclinic, space group $P\bar{1}$, with $a = 10.642(2)$, $b = 12.771(3)$, $c = 9.430(1)$ Å, $\alpha = 89.69(1)$, $\beta = 104.03(1)$, $\gamma = 96.97(2)°$, and $Z = 2$. The average bond distances Fe–N 1.970 and Fe–O 1.895 Å are in good agreement with the corresponding values reported for low-spin isomers of other spin-crossover iron(III) complexes.

A spin-equilibrium phenomenon between high-spin and low-spin states has been confirmed by the application of Mössbauer, e.s.r., *X*-ray photoelectron, and i.r. spectroscopy since Cambi *et al.*[1] and Ewald *et al.*[2] first observed magnetic isomerism for tris(dithiocarbamato)iron(III). A number of spin-crossover complexes of Fe^{III}, Fe^{II}, and Co^{III} have so far been reported.[3–7] In the case of the spin-crossover phenomenon observed in the solid state, the complexes can be, in general, classified into two groups according to the thermodynamical behaviour of spin transition. (I) The complexes of the first group show dynamic spin equilibrium, the interconversion between high-spin and low-spin states. Recently iron(III) compounds that flip spin at a rate faster than the ^{57}Fe Mössbauer time-scale have been reported.[8–11] A smooth increase of magnetic moments with temperature is observed for the complexes. (II) The complexes of the second group show transition of the spin state depending on temperature. The transition of this type may be connected with a first-order phase transition in the solid state from long-range electron–phonon coupling.[12] We may refer to case (I) as 'spin equilibrium', while case (II) may be named 'spin transition'. This distinction, however, does not mean that the whole phenomenon must originate from different mechanisms.

The dynamic behaviour over a period of time of the order of 10^{-6} s—10^{-8} s in the first group can be studied in the solid state for iron compounds using Mössbauer spectroscopy because the lifetime of ^{57m}Fe is 1×10^{-7} s. The nucleus of an iron atom which shows fast electronic relaxation between high-spin and low-spin states 'sees' an average of the properties of both states,

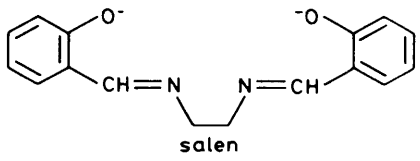

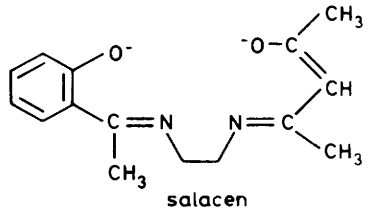

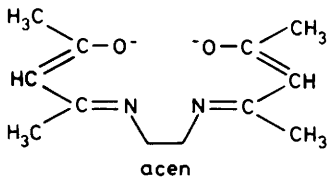

and the values of the Mössbauer parameters are averaged and depend on the population of each state. In this paper we propose a time-dependent Hamiltonian which represents a reasonable physical model, and by using the Hamiltonian, the spin-interconversion rates have been calculated from the Mössbauer lineshape.

Iron(III) complexes of *NN'*-ethylenebis(salicylideneiminate) (salen) are all high-spin if a cyanide ion is not co-ordinated and some of the iron(III) complexes of *NN'*-ethylenebis(acetylacetonylideneiminate) (acen) are spin-crossover complexes which show fast spin conversion.[8] The ligand salacen is intermediate between acen and salen in chemical structure. In general, spin transition between high-spin and low-spin states is accompanied by changes in metal–ligand bond length.[13–16] In this paper the magnetic and spectroscopic properties of the

† [Ethylene(*N*-acetylacetonylideneiminato)(*N'*-α-methylsalicylideneiminato)]bis(imidazole)iron(III) hexafluorophosphate.

Supplementary data available (No. SUP 56495, 5 pp.): H-atom co-ordinates, thermal parameters. See Instructions for Authors, *J. Chem. Soc., Dalton Trans.*, 1986, Issue 1, pp. xvii—xx. Structure factors are available from the editorial office.

Non-S.I. units employed: B.M. ≈ 9.274×10^{-24} J T^{-1}; eV ≈ 1.60×10^{-19} J.

complexes which show faster spin-interconversion rates than the lifetime of the excited state of ^{57}Fe and how spin interconversion is influenced by the chemical structure of ligands have been examined.

Experimental

The magnetic susceptibility data on the polycrystalline samples at various temperatures (80—310 K) were obtained by the Faraday method, using an instrument described earlier.[8] The magnetic susceptibilities were calibrated with $Hg[Co(NCS)_4]$, corrected for the diamagnetism of the ligands and anions, and the effective magnetic moments were calculated by the formula $\mu_{eff.} = 2.83(\chi_M T)^{\frac{1}{2}}$, where χ_M is the corrected molar magnetic susceptibility and T the temperature in K.

Mössbauer spectroscopy was effected by using an instrument described elsewhere.[8] All isomer shifts are reported with respect to the centroid of the spectrum of iron foil enriched with ^{57}Fe at 295 K. The spectra were fitted to the Lorentzian line shapes by using a least-squares method at the Computer Centre, Kyushu University. The electronic spectra in dichloromethane solution were recorded on a Hitachi 340 spectrophotometer, where the temperature of a sample solution was thermostatted within ±0.1 °C using a temperature-controlled circulating bath (Neslab RTE-8).

Compound Preparation.—Schiff-base ligands were prepared by the demetallation reaction of corresponding copper(II) complexes with gaseous hydrogen sulphide in dichloromethane solution, according to the method reported earlier.[17]

Preparation of $[Fe(Him)_2(salacen)]PF_6$.—A mixture of [FeCl(salacen)] [salacen = ethylene(*N*-acetylacetonylideneiminate)(*N'*-α-methylsalicylideneiminate)] (5 mmol) and imidazole (Him) (10 mmol) in absolute methanol (100 cm^3) was stirred at 50 °C for 30 min, and the solution was filtered while hot. The filtrate was added to a solution of sodium hexafluorophosphate (5 mmol) in absolute methanol (10 cm^3). The solution was allowed to stand overnight to precipitate black crystals. The crystals were recrystallized from a mixture of dichloromethane and absolute methanol (Found C, 42.55; H, 4.35; N, 14.0. Calc. for $C_{21}H_{26}F_6FeN_6O_2P$: C, 42.4; H, 4.40; N, 14.15%). The preparative method for the *N*-methylimidazole (mim) complex $[Fe(mim)_2(salacen)]PF_6$ is similar to that above (Found: C, 44.5; H, 4.90; N, 13.5. Calc. for $C_{23}H_{30}F_6FeN_6O_2P$: C, 44.35; H, 4.80; N, 13.5%).

Crystal Structure Determination of $[Fe(Him)_2(salacen)]PF_6$.—Suitable single crystals of $[Fe(Him)_2(salacen)]PF_6$ were obtained by slow evaporation of a mixture of dichloromethane and methanol at ambient temperature.

Crystal data. $C_{21}H_{26}F_6FeN_6O_2P$, $M = 593.3$, triclinic system, space group $P\bar{1}$, $Z = 2$, $a = 10.642(2)$, $b = 12.771(3)$, $c = 9.430(1)$ Å, $\alpha = 89.69(1)$, $\beta = 104.03(1)$, $\gamma = 96.97(2)°$, $U = 1\,233.9(5)$ Å^3, $D_c = 1.597$ g cm^{-3}, $D_m = 1.59$ g cm^{-3}, $F(000) = 610$, $\mu = 7.7$ cm^{-1}, crystal dimensions 0.4 × 0.5 × 0.5 mm.

Diffraction data were collected at 293 ± 1 K on a Rigakudenki AFC-5 four-circle diffractometer at the Institute for Molecular Science, using graphite-monochromatized Mo-K_α radiation ($\lambda = 0.710\,73$ Å). Lattice parameters and their standard deviations were obtained from a least-squares fit to 50 values of 2θ in the range $20 < 2\theta < 30°$. For the intensity data collection, a θ–2θ scan mode was used at a scan rate of 3° min^{-1}. The intensities of three standard reflections, monitored every 100 reflections, showed no greater fluctuations during the data collection than those expected from Poisson statistics. The raw intensity data of 3 237 reflections were collected in the range

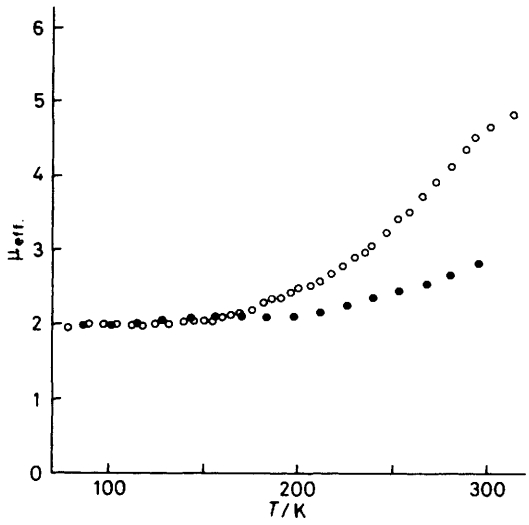

Figure 1. Temperature dependences of the effective magnetic moment ($\mu_{eff.}$) for $[Fe(Him)_2(salacen)]PF_6$ (●) and $[Fe(mim)_2(salacen)]PF_6$ (○)

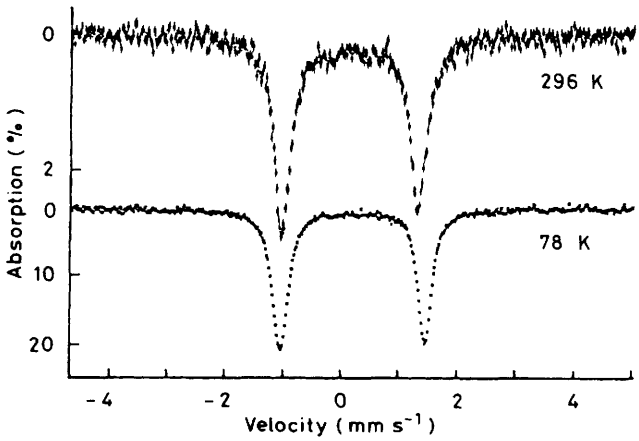

Figure 2. Mössbauer spectra of $[Fe(Him)_2(salacen)]PF_6$ at 78 and 296 K

$1.5 < 2\theta < 44°$, of which 2 563 independent reflections with $|F_o| > 3\sigma(|F_o|)$ were used for the structure determination. The intensity data were corrected for Lorentz-polarization effects, but not for absorption.

Solution and refinement of the structure. Determination of structural parameters was carried out with the Universal Crystallographic Computation Program System UNICS III,[18] using a HITAC M-200H Computer at the Computer Centre of the Institute for Molecular Science. Atomic scattering factors for non-hydrogen atoms were taken from ref. 19 and those for hydrogen atoms from Stewart *et al.*[20] The effects of anomalous dispersion for non-hydrogen atoms were corrected for in the structure factor calculations. The structure was solved by the conventional heavy-atom method and refined by a block-diagonal least-squares method. Reliability factors are defined as $R = \Sigma||F_o| - |F_c||/\Sigma|F_o|$ and $R' = [\Sigma w(|F_o| - |F_c|)^2/\Sigma w|F_o|^2]^{\frac{1}{2}}$. The weighting scheme $w = [\sigma_c^2 + (0.015|F_o|)^2]^{-1}$ was employed, where $\sigma_c = (\bar{N})^{\frac{1}{2}}$ is a counting statistics error with Gaussian distribution function $\rho(N) = (2\pi\bar{N})^{-\frac{1}{2}}\exp[-(N - \bar{N})^2/2\bar{N}]$. The position of the iron atom was determined from three-dimensional Patterson functions and successive Fourier syntheses located all the non-hydrogen atoms except for the fluorine atoms of the PF_6^- anion. The fluorine atoms were

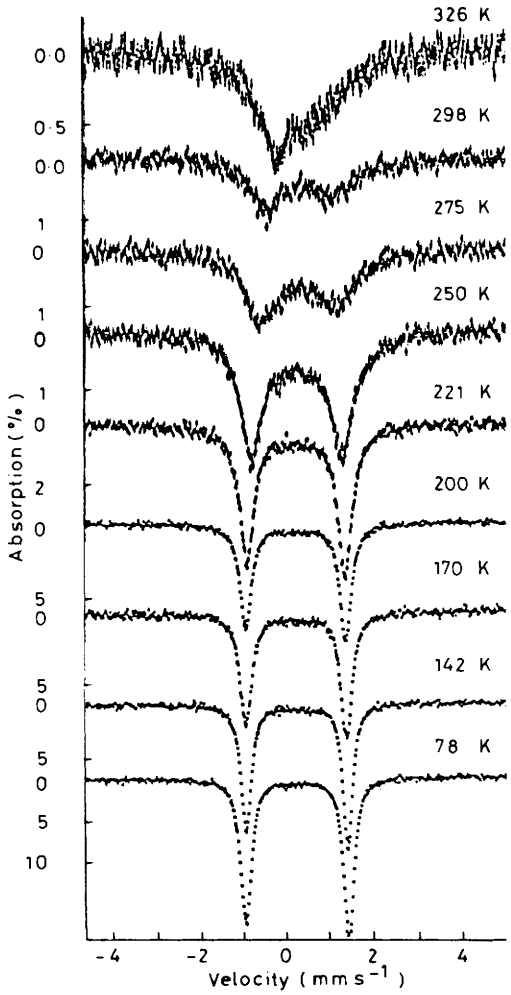

Figure 3. Temperature dependence of the Mössbauer spectra of $[Fe(mim)_2(salacen)]PF_6$

subjected to a disorder, and the occupancy factors were assigned to the twelve possible positions located in the difference Fourier map according to the peak heights. Refinement was carried out by introducing anisotropic thermal parameters for all the non-hydrogen atoms except for fluorine and isotropic parameters for these. Hydrogen atoms were inserted at calculated positions and included for the structure factor calculations. The final indices R and R' were 0.0919 and 0.1144, respectively.

Results and Discussion

Magnetic Properties.—The temperature dependences of magnetic moments for both compounds were examined and the results are illustrated in Figure 1. No hysteresis was detected. It is clear from Figure 1 that $[Fe(Him)_2(salacen)]PF_6$ is essentially a low-spin isomer in the solid state at room temperature. On the other hand, $[Fe(mim)_2(salacen)]PF_6$ is in the high-spin state at 300 K and the electronic state changes to the low-spin state with decreasing temperature. The magnetic behaviour is characteristic of a high-spin $\rightleftharpoons$ low-spin interconversion process.

Mössbauer Spectra.—Figure 2 shows the Mössbauer spectra for $[Fe(Him)_2(salacen)]PF_6$, from which the Mössbauer quadrupole splitting, Δ = 2.352 mm s^{-1}, and isomer shift, δ = 0.167 mm s^{-1}, and Γ_{hi} = 0.378 mm s^{-1} and Γ_{lo} = 0.348 mm s^{-1} are obtained. These values are in accordance with the magnetic susceptibility data. The variable-temperature Mössbauer spectra for $[Fe(mim)_2(salacen)]PF_6$ are shown in Figure 3, which serve to characterize the anomalous magnetic properties as arising from spin interconversion. Mössbauer data for $[Fe(mim)_2(salacen)]PF_6$ are listed in Table 1, where the spectra are fitted to one doublet or two doublets with Lorentzian peaks. The spectrum at 326 K exhibits only a broad high-spin iron(III) absorption. Spectra for bulky high-spin iron(III) complexes ($^6A_{1g}$) are often asymmetric and broad due to spin–spin and/or weak spin–lattice interactions. At 78 K a low-spin doublet with Δ = 2.368 mm s^{-1} is observed in the spectrum in accordance with the magnetic data. The spectrum at 250 K can be fitted to two doublets of Lorentzian peaks, one for the high-spin and the other for low-spin isomer. It is obvious that in this temperature range (78—250 K) the molecules of the compound show interconversion between high-spin and low-spin states slower than 10^6 s^{-1}. The Mössbauer spectrum at 275 K shows a single doublet, each peak having a broad full-width at half-maximum (f.w.h.m.), 0.861 mm s^{-1} (lower energy peak) and 1.161 mm s^{-1} (higher energy peak), which cannot be fitted to two doublets of the high-spin and low-spin isomers. A population of high-spin isomer (x) at a certain temperature is obtained by assuming simple additive properties for the magnetic susceptibilities [$\mu^2 = x\mu_h^2 + (1 - x)\mu_l^2$]. The high-spin population x = 0.09 is estimated from the absorption area of the Mössbauer spectra at 250 K. This is not in accordance with x = 0.24 estimated from the magnetic susceptibilities, if the values of μ_l = 2.0 B.M. and μ_h = 5.8 B.M. are taken. This disagreement shows that fitting relaxation spectra with intermediate spin-interconversion rates to two doublets (high-spin and low-spin isomers) is not good. Centre shifts of Mössbauer lines normally decrease with increasing temperature by virtue of the second-order Doppler shift. Above 275 K, the spectra are characterized by line broadening and inward coalescence. A small temperature dependence of Δ is expected for low-spin compounds as shown in the spectra of $[Fe(Him)_2(salacen)]PF_6$. It should be noted that the centroids of the two doublets seem to converge toward the same velocity and increase above 250 K as the temperature is raised. Spin-interconversion rates become fast when the temperature is

Table 1. Mössbauer data for $[Fe(mim)_2(salacen)]PF_6$

T/K	δ^a	Δ^a	$\Gamma_{lo}{}^{a,b}$	$\Gamma_{hi}{}^{a,c}$	$A_{lo}{}^d$	$A_{hi}{}^e$	A^f	s.s.w.r.^{g}
(*a*) Fitting the spectra to one doublet								
78	0.236	2.368	0.287	0.278	4.463	4.816	9.279	641
100	0.232	2.359	0.281	0.261	3.971	4.259	8.230	671
122	0.227	2.344	0.279	0.264	3.422	3.697	7.119	505
142	0.221	2.336	0.277	0.258	2.780	3.000	5.780	508
170	0.212	2.310	0.327	0.311	2.189	2.381	4.570	599
200	0.208	2.293	0.327	0.321	1.866	2.103	3.969	755
221	0.208	2.237	0.434	0.436	1.615	1.787	3.402	834
250	0.219	2.184	0.741	0.939	1.268	1.507	2.775	1 087
275	0.265	1.703	0.861	1.161	0.855	0.903	1.758	521
299	0.267	1.470	0.882	1.386	0.608	0.708	1.316	502
326	0.294	1.232	0.960	1.506	0.400	0.385	0.785	446
(*b*) Fitting the spectra to two doublets								
250	0.200	0.517	0.484	0.484	0.111	0.111	0.222	662
	0.228	2.063	0.595	0.696	1.066	1.193	2.259	

^{a} Units are mm s^{-1}. ^{b} F.w.h.m. for the lower energy line. ^{c} F.w.h.m. for the higher energy line. ^{d} Absorption area for the lower energy line. ^{e} Absorption area for the higher energy line. ^{f} Total absorption area under the curve. ^{g} Sum of the square of the weighted residuals.

raised and the nucleus of an iron atom 'sees' an average of the properties of the high-spin and low-spin electronic states. The reason that the values of χ^2 are larger than the degree of freedom below 250 K is due to faint residual high-spin impurities or the high-spin isomer, in view of the magnetic susceptibility data.

Simulation of the Mössbauer Spectra of Spin-crossover Complexes.—A quantum mechanical theory of narrowing of spectral lines by exchange or motion has been derived by Anderson and Weiss,[21] by Kubo,[22] by Kubo and Tomita,[23] and by Sack.[24] An application of the stochastic model to Mössbauer spectra has been developed by Blume and Tjon.[25,26] If such stochastic Hamiltonians (random function of time) are considered, the observed probability of emission of a photon $\boldsymbol{k}$ is the stochastic average of the expression (1),[25] where $[]_{av}$ denotes the average over the stochastic degrees of freedom in the Hamiltonian, $\mathscr{H}^{(+)}(t)$ a time-dependent Hamiltonian for the nucleus, $\mathscr{H}^{(-)} = \mathscr{H}^{(+)\dagger}$, i = imaginary number, Γ = inverse of the natural lifetime of the excited state, and t = time.

Stochastic model (I). This is the case where the sign of the electric field gradient (e.f.g.) of the high-spin state is the same as that of the low-spin state.

We wish to give a Hamiltonian for a nucleus in an e.f.g. which jumps at random between the high-spin and low-spin states. We introduce a random function of time, f(t) which takes two possible values, ± 1.

The Hamiltonian may be written as in equation (2), where $\mathscr{H}_0$ is the Hamiltonian for the nucleus in the absence of any perturbations, I the nuclear spin operator ($I = \frac{3}{2}$), and Q_l and Q_h are $\frac{1}{12}\Delta_l$ and $\frac{1}{12}\Delta_h$; Δ_l and Δ_h are the quadrupole splittings for the high-spin and low-spin states. Equation (2) becomes (3) when f(t) = 1 reduces to $\mathscr{H}_0 + \frac{1}{6}\Delta_l(3I_z^2 - I^2)$, while f($t$) = −1 yields $\mathscr{H}_0 + \frac{1}{6}\Delta_h(3I_z^2 - I^2)$, where $q_1 = Q_l + Q_h = \frac{1}{12}(\Delta_l + \Delta_h)$ and $q_2 = Q_l - Q_h = \frac{1}{12}(\Delta_l - \Delta_h)$. If we consider a nucleus with an excited state of spin $I_1 = \frac{3}{2}$ and a ground state of spin $I_0 = \frac{1}{2}$, we have equation (4) where $U^\dagger(t) = \exp[i\int_0^t \mathscr{H}(t')dt']$ and $U(t) = \exp[-i\int_0^t \mathscr{H}(t')dt']$, and $|I_1 m_1>$ and $|I_0 m_0>$ are the excited and ground state of the nucleus, respectively. An $I_0 = \frac{1}{2}$ state has no effect in the I_0 matrix element, and we can therefore write equation (5) where δ is Kronecker's delta.

If we consider the probability of emission from a powder, we need only the diagonal element of equation (5). Under this restriction, this gives equation (6). For ^{57}Fe, $E_1 - E_0 = 14.4$ keV. The main calculation of the equation (6) is to evaluate the average $\{\exp[-iq_2(3m_1^2 - \frac{15}{4})\int_0^t f(t')dt']\}_{av}$. However, the solution of equation (6) has been given by Abragam[27] as shown by equation (7) where $\alpha = q_2(3m_1^2 - \frac{15}{4})$ and p_i is the population for state i. This gives equation (8), where $\omega_0 = E_1 - E_0$ is the frequency of the unsplit line. If we define $G_{m_1}(p)$ as in equation (9) this leads to equation (10). Performing the integration in $G_{m_1}(p)$ yields[25] equation (11) where $p = -i\{\omega - \omega_0 - q_1(3m_1^2 - \frac{15}{4})\} + \frac{1}{2}\Gamma$; $\boldsymbol{W}$ is the matrix of transition

$$\boldsymbol{W} = \begin{pmatrix} -W_l & W_l \\ W_h & -W_h \end{pmatrix} \qquad \boldsymbol{F} = \begin{pmatrix} 1 & 0 \\ 0 & -1 \end{pmatrix}$$

probabilities per unit time between the two values of f(t) with diagonal elements determined by $W_{ii} = -\sum_i W_{ij}(j \neq i)$ and $\boldsymbol{F}$ is the matrix whose diagonal elements are the permissible values of f(t).

Finally we have equation (12), where $p_l W_l = p_h W_h$ and $p_l + p_h = 1$. Parameters p_h and p_l are fractions of the high-spin and low-spin isomers, respectively. The real part of $G_{m_1}(p)$ gives line shape for variable relaxation times between the high spin and low-spin states. A representative example is shown in Figure 4.

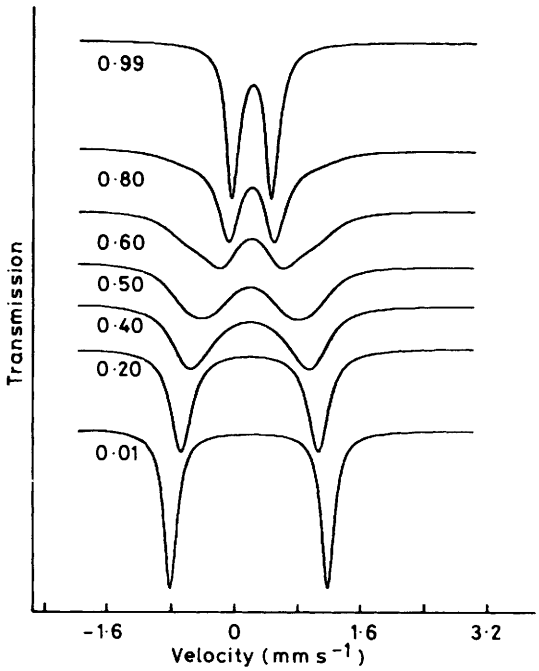

Figure 4. Theoretical lineshapes (values of p_h given) for spin interconversion between high-spin and low-spin states using the following parameters: $\Delta_l = -2.00$, $\Delta_h = +0.50$, $\delta = 0.20$, $\Gamma = 0.20$ mm s^{-1}, and $\tau_l = 3 \times 10^{-7}$ s

Stochastic model (II). In this case the sign of the e.f.g. of the low-spin state is the reverse of that of the high-spin state.

In the case that the e.f.g. of the high-spin state is perpendicular to that of the low-spin state, the Hamiltonian may be written as equation (13), where $Q_l = \Delta_l/6$, $Q_h = \Delta_h/6$, f(t) = ± 1, $q_1 = Q_l/2 + Q_h/4$, $q_2 = Q_l/2 - Q_h/4$, and $q_3 = 3Q_h/8$. Combining equation (13) with equation (1) gives equation (14), where $\mathscr{H}_1(t) = [q_2 + q_1 f(t)](3I_z^2 - I^2)$ and $V(t) = [1 - f(t)]q_3(I_+^2 + I_-^2)$. Considering the calculation[26] of $G_m(t)$, equation (15), writing equations (16) and (17), and expanding exponential terms in a time-ordered series, we obtain equation (18). Since $V(t)$ has the selection rule $\Delta m = \pm 2$, the matrix elements with n odd in equation (18) vanish. Writing equation (19), where $f_1(t) = q_2 + q_1 f(t)$ and $\beta = -(3m_1^2 - \frac{15}{4})$, and further, equation (20), gives equation (21).

If we introduce next equations (22) and (23), equation (21) can be written as equation (24). Accordingly, we have equation (25). Taking the Laplace transformation of $G_{m_1}(t)$,[26] we have equations (26) and (27), where $p = -i(\omega - \omega_0) + \frac{1}{2}\Gamma$, $\tilde{A}(p) = (p - i\beta\boldsymbol{F}_1 - \boldsymbol{W})^{-1}$, $\tilde{B}(p) = \boldsymbol{F}(p + i\beta\boldsymbol{F}_1 - \boldsymbol{W})^{-1}\boldsymbol{F}$, and $\boldsymbol{F}$, $\boldsymbol{F}_1$, and $\boldsymbol{W}$ are as given below.

$$\boldsymbol{F}_1 = \begin{pmatrix} q_2 + q_1 & 0 \\ 0 & q_2 - q_1 \end{pmatrix} \quad \boldsymbol{F} = \begin{pmatrix} 0 & 0 \\ 0 & 2 \end{pmatrix} \quad \boldsymbol{W} = \begin{pmatrix} -W_l & W_l \\ W_h & -W_h \end{pmatrix}$$

Finally we obtain equation (28), where $a = p + 3i(q_2 - q_1) + W_h$, $b = p + 3i(q_2 + q_1) + W_l$, $c = p - 3i(q_2 + q_1) + W_l$, and $d = p - 3i(q_2 - q_1) + W_h$. The real part of $G_{m_1}(p)$ gives a shape for variable relaxation times between the high-spin and low-spin states.

A nucleus 'sees' the average of the e.f.g between the high-spin

$$W(\boldsymbol{k}) = (2/\Gamma)\ Re\int_0^\infty \mathrm{d}t\ \exp\ (i\omega t - \tfrac{1}{2}\Gamma t)[\langle \mathscr{H}^{(-)}\mathscr{H}^{(+)}(t)\rangle]_{\mathrm{av}} \tag{1}$$

$$\mathscr{H} = \mathscr{H}_0 + \{[1 + \mathrm{f}(t)]Q_\mathrm{l} + [1 - \mathrm{f}(t)]Q_\mathrm{h}\}(3I_z^2 - I^2) \tag{2}$$

$$\mathscr{H} = \mathscr{H}_0 + [q_1 + q_2\mathrm{f}(t)]\,(3I_z^2 - I^2) \tag{3}$$

$$[\langle \mathscr{H}^{(-)}\mathscr{H}^{(+)}(t)\rangle]_{\mathrm{av}} = \frac{1}{2I_\mathrm{l} + 1}\sum_{m_0m_\mathrm{l}m_0'm_\mathrm{l}'}[\langle I_\mathrm{l}m_\mathrm{l}|\mathscr{H}^{(-)}|I_0m_0\rangle\langle I_0m_0|U^\dagger(t)|I_0m_0'\rangle\langle I_0m_0'|\mathscr{H}^{(+)}|I_\mathrm{l}m_\mathrm{l}'\rangle\langle I_\mathrm{l}m_\mathrm{l}'|U(t)|I_\mathrm{l}m_\mathrm{l}\rangle]_{\mathrm{av}} \tag{4}$$

$$\langle I_0m_0|U^\dagger(t)|I_0m_0'\rangle = \exp(iE_0t)\delta_{m_0m_0'};\ \langle I_\mathrm{l}m_\mathrm{l}'|U(t)|I_\mathrm{l}m_\mathrm{l}\rangle = \exp\{-i[E_\mathrm{l}t + q_1(3I_z^2 - I^2)t + q_2(3I_z^2 - I^2)\int_0^t \mathrm{f}(t')\mathrm{d}t']\}\delta_{m_\mathrm{l}m_\mathrm{l}'} \tag{5}$$

$$[\langle \mathscr{H}^{(-)}\mathscr{H}^{(+)}(t)\rangle]_{\mathrm{av}} = \tfrac{1}{4}\sum_{m_0m_\mathrm{l}}|\langle I_0m_0|\mathscr{H}^{(+)}|I_\mathrm{l}m_\mathrm{l}\rangle|^2\exp[-i(E_\mathrm{l} - E_0)t - iq_1(3m_\mathrm{l}^2 - \tfrac{15}{4})t]\{\exp[-iq_2(3m_\mathrm{l}^2 - \tfrac{15}{4})\int_0^t \mathrm{f}(t')\mathrm{d}t']\}_{\mathrm{av}} \tag{6}$$

$$\{\exp[-i\alpha\int_0^t \mathrm{f}(t')\mathrm{d}t']\}_{\mathrm{av}} = \sum_{ij}p_i\{j|\exp[(-i\alpha\boldsymbol{F} + \boldsymbol{W})t]|i\} \tag{7}$$

$$W(\boldsymbol{k}) = \frac{1}{2\Gamma}\ Re\sum_{m_0m_\mathrm{l}}|\langle I_0m_0|\mathscr{H}^{(+)}|I_\mathrm{l}m_\mathrm{l}\rangle|^2\int_0^\infty \mathrm{d}t\ \exp[-\mathrm{i}\{\omega_0 - \omega + q_1(3m_\mathrm{l}^2 - \tfrac{15}{4})\}t - \tfrac{1}{2}\Gamma t]\ \sum_{ij}p_i\{j|\exp[(-i\alpha\boldsymbol{F} + \boldsymbol{W})t]|i\} \tag{8}$$

$$G_{m_\mathrm{l}}(p) = \int_0^\infty \mathrm{d}t\ \exp\{-i[\omega_0 - \omega + q_1(3m_\mathrm{l}^2 - \tfrac{15}{4})]t - \tfrac{1}{2}\Gamma t\}\sum_{ij}p_i\{j|\exp[(-i\alpha\boldsymbol{F} + \boldsymbol{W})t]|i\} \tag{9}$$

$$W(\boldsymbol{k}) = \frac{1}{2\Gamma}\ Re\sum_{m_0m_\mathrm{l}}|\langle I_0m_0|\mathscr{H}^{(+)}|I_\mathrm{l}m_\mathrm{l}\rangle|^2G_{m_\mathrm{l}}(p) \tag{10}$$

$$G_{m_\mathrm{l}}(p) = \sum_{ij}p_i[j|(p - \boldsymbol{W} + i\alpha\boldsymbol{F})^{-1}|i] \tag{11}$$

$$G_{m_\mathrm{l}}(p) = \frac{p_\mathrm{l}(p - i\alpha + W_\mathrm{l} + W_\mathrm{h}) + p_\mathrm{h}(p + i\alpha + W_\mathrm{l} + W_\mathrm{h})}{(p + i\alpha + W_\mathrm{l})(p - i\alpha + W_\mathrm{h}) - W_\mathrm{l}W_\mathrm{h}} \tag{12}$$

$$\mathscr{H} = \mathscr{H}_0 + \frac{Q_\mathrm{l}}{2}[1 + \mathrm{f}(t)](3I_z^2 - I^2) + \frac{Q_\mathrm{h}}{2}[1 - \mathrm{f}(t)](3I_x^2 - I^2) = \mathscr{H}_0 + \left[\frac{Q_\mathrm{l}}{2} - \frac{Q_\mathrm{h}}{4} + \left(\frac{Q_\mathrm{l}}{2} + \frac{Q_\mathrm{h}}{4}\right)\mathrm{f}(t)\right](3I_z^2 - I_2) +$$

$$\tfrac{3}{8}Q_\mathrm{h}[1 - \mathrm{f}(t)](I_+^2 + I_-^2) = \mathscr{H}_0 + [q_2 + q_1\mathrm{f}(t)](3I_z^2 - I^2) + q_3[1 - \mathrm{f}(t)](I_+^2 + I_-^2) \tag{13}$$

$$W(\boldsymbol{k}) = \frac{2}{\Gamma}\ Re\int_0^\infty \mathrm{d}t\ \exp\{i(\omega - \omega_0)t - \tfrac{1}{2}\Gamma t\}[\tfrac{1}{4}\sum_{m_0m_\mathrm{l}}|\langle I_0m_0|\ \mathscr{H}^{(+)}|I_\mathrm{l}m_\mathrm{l}\rangle|^2][\langle I_\mathrm{l}m_\mathrm{l}|\exp\{-i\int_0^t [\mathscr{H}_\mathrm{l}(t') + V(t')]\mathrm{d}t'\}|I_\mathrm{l}m_\mathrm{l}\rangle]_{\mathrm{av}} \tag{14}$$

$$G_{m_\mathrm{l}}(t) = [\langle I_\mathrm{l}m_\mathrm{l}|\exp\{-i\int_0^t [\mathscr{H}_\mathrm{l}(t') + V(t')]\mathrm{d}t'\}|I_\mathrm{l}m_\mathrm{l}\rangle]_{\mathrm{av}} \tag{15}$$

$$\exp\{-i\int_0^t [\mathscr{H}_\mathrm{l}(t') + V(t')]\mathrm{d}t'\} = \exp[-i\int_0^t \mathscr{H}_\mathrm{l}(t')\mathrm{d}t']\exp[-i\int_0^t \bar{V}(t')\mathrm{d}t'] \tag{16}$$

$$\bar{V}(t) = \exp[i\int_0^t \mathscr{H}_\mathrm{l}(t')\mathrm{d}t']V(t)\exp[-i\int_0^t \mathscr{H}_\mathrm{l}(t')dt'] \tag{17}$$

$$G_{m_\mathrm{l}}(t) = \sum_n(-i)^n\int_0^t \mathrm{d}t_1\cdots\int_0^{t_{n-1}}\mathrm{d}t_n\{\langle I_\mathrm{l}m_\mathrm{l}|\ \exp[-i\int_0^t \mathscr{H}_\mathrm{l}(t')\mathrm{d}t']\bar{V}(t_1)\cdots\ \bar{V}(t_n)|I_\mathrm{l}m_\mathrm{l}\rangle\}_{\mathrm{av}} \tag{18}$$

$$\Psi_{2n} = \langle I_\mathrm{l}m_\mathrm{l}|\exp[-i\int_0^t \mathscr{H}_\mathrm{l}(t')\mathrm{d}t']\bar{V}(t_1)\cdots\ \bar{V}(t_{2n})|I_\mathrm{l}m_\mathrm{l}\rangle = \exp\{-i(3m_\mathrm{l}^2 - \tfrac{15}{4})\int_0^t [q_2 + q_1\ \mathrm{f}(t')]\mathrm{d}t'\}\ \times$$

$$\langle I_\mathrm{l}m_\mathrm{l}|\bar{V}(t_1)\bar{V}(t_2)|I_\mathrm{l}m_\mathrm{l}\rangle\cdots\langle I_\mathrm{l}m_\mathrm{l}|\bar{V}(t_{2n-1})\bar{V}(t_{2n})|I_\mathrm{l}m_\mathrm{l}\rangle = \exp[i\beta\int_0^t \mathrm{f}_\mathrm{l}(t')\mathrm{d}t']\ \langle I_\mathrm{l}m_\mathrm{l}|\bar{V}(t_1)\bar{V}(t_2)|I_\mathrm{l}m_\mathrm{l}\rangle\cdots$$

$$\langle I_\mathrm{l}m_\mathrm{l}|\bar{V}(t_{2n-1})\bar{V}(t_{2n})|I_\mathrm{l}m_\mathrm{l}\rangle \tag{19}$$

$$\langle I_1 m_1|\bar{V}(t_1)\bar{V}(t_2)|I_1 m_1\rangle = \exp[-i\beta\int_0^{t_1} f_1(t')dt'][1 - f(t_1)]\exp[-i\beta\int_0^{t_1} f_1(t')dt']\exp[i\beta\int_0^{t_2} f_1(t')dt'] \times$$
$$[1 - f(t_2)]\exp[i\beta\int_0^{t_2} f_1(t')dt']q_3^2|\langle I_1 m_1|I_+^2|I_1 m_1 - 2\rangle|^2 \quad (20)$$

$$\psi_{2n} = (12\,q_3^2)^n\exp[i\beta\int_{t_1}^{t} f_1(t')dt'][1 - f(t_1)]\exp[-i\beta\int_{t_2}^{t_1} f_1(t')dt'][1 - f(t_2)]\cdots[1 - f(t_{2n})]\exp(i\beta\int_0^{t_{2n}} f_1(t')dt'] \quad (21)$$

$$[j|A(t_n - t_{n'})|i] = \exp[i\beta\int_{t_{n'}}^{t_n} f_1(t')dt'] \quad (22)$$

$$[j|B(t_n - t_{n'})|i] = (1 - f_n)\exp[-i\beta\int_{t_{n'}}^{t_n} f_1(t')dt'](1 - f_{n'}) \quad (23)$$

$$\psi_{2n} = \sum_{ij} p_i[j|(12\,q_3^2)^n A(t - t_1)B(t_1 - t_2)\cdots B(t_{2n-1} - t_{2n})A(t_{2n})|i] \quad (24)$$

$$G_{m_1}(t) = \sum_{ij} p_i[j|\sum_n (-12\,q_3^2)^n\int_0^t dt_1\cdots\int_0^{t_{2n-1}} dt_{2n}A(t - t_1)B(t_1 - t_2)\cdots B(t_{2n-1}t_{2n})A(t_{2n})|i] \quad (25)$$

$$G_{m_1}(p) = \int_0^\infty dt\,\exp(-pt)G_{m_1}(t) = \sum_{ij} p_i\{j|[\tilde{A}(p)^{-1} + (12\,q_3^2)\tilde{B}(p)]^{-1}|i\} \quad (26)$$

$$W(\boldsymbol{k}) = \frac{1}{2\Gamma}\,Re\sum_{m_0 m_1}|\langle I_0 m_0|\mathscr{H}^{(+)}|I_1 m_1\rangle|^2\sum_{ij} p_i\{j|[\tilde{A}(p)^{-1} + (12\,q_3^2)\tilde{B}(p)]^{-1}|i\} \quad (27)$$

$$G_{m_1}(p) = \frac{1}{c[d + 48bq_3^2/(ab - W_1W_h)] - W_1W_h}\left[p_l\left(d + \frac{48bq_3^2}{ab - W_1W_h} + W_1\right) + p_h(W_h + c)\right] +$$
$$\frac{1}{b[a + 48cq_3^2/(cd - W_1W_h)] - W_1W_h}\left[p_l\left(a + \frac{48cq_3^2}{cd - W_1W_h} + W_1\right) + p_h(W_h + b)\right] \quad (28)$$

and low-spin states in the limit of fast relaxation. Figure 5 shows the variation of the quadrupole splitting *vs.* the fraction of high-spin isomer; the quadrupole splitting values change linearly with the fraction of high-spin isomer in the case where the signs of the e.f.g. for the high-spin and low-spin states are the same. On the other hand, it should be noted that the variation of quadrupole splittings experiences a minimum point in the case where the sign of the e.f.g. for the high-spin state is the reverse from that of the low-spin state. It is concluded that the behaviour of the temperature dependence of the quadrupole splitting gives information about the sign of the e.f.g. of both electronic states of the spin-crossover complexes. Wickman's equation [28] is widely used for relaxation processes and it gives good resolution for the case where the main axes of the e.f.g. are parallel or antiparallel to each other. In these models good resolution is given for the case in which the isomer shift of one state is similar to that of the other and the main axes of the e.f.g. are parallel or antiparallel to each other.

The stochastic model (I) was applied to the spectra of $[Fe(mim)_2(salacen)]PF_6$ because the isomer shift (δ) values of the high-spin and low-spin isomers for the complex are observed in the region *ca.* 0.2—0.3 mm s^{-1}; the difference is small and the quadrupole splitting (Δ) values decrease linearly on increasing temperature. In our model, it is supposed that the relaxation process occurs between high-spin and low-spin states having the same δ values and same linewidths. The parameters $\Delta_l = 2.36$, $\Delta_h = 1.00$, and $\Gamma = 0.28$ mm s^{-1} were taken in the simulation. In fitting the experimental spectra to this model the δ values are taken from the experimental data and the populations of the high-spin isomers were taken from the magnetic susceptibility data. The computer minimizations of equation (12) result in the theoretical spectra presented in Figure 6. The value of correlation time τ is defined as $\tau_l\tau_h/(\tau_l + \tau_h)$, where τ_h and τ_l are the lifetimes calculated from computer minimization for the high-spin and low-spin isomers respectively. The fit is good only at low temperatures because the increase of the ^6A state population makes the linewidth broad owing to both the spin–spin and spin–lattice relaxations. Therefore, the relaxation times calculated for this complex may be convincing only at low temperatures. However, simulating Mössbauer spectra with a time-dependent Hamiltonian is the only means of determining a spin-interconversion rate in the solid state. The observed relaxation times τ span a range from 0.15 to 0.32 μs and are dependent on temperature. It should be noted that $[Fe(mim)_2(salacen)]PF_6$ is one of the rare complexes which show fast spin interconversion. Although it is reported that the spin-conversion processes lie in the normal free-energy region of classical activated-complex theory (corresponds to the very strong coupling case of radiationless transition theory),[29,30] it will be important to determine by what process the fast spin transition proceeds.

Crystal and Molecular Structure of $[Fe(Him)_2(salacen)]PF_6$.—Positional parameters for non-hydrogen atoms are given in Table 2. Figure 7 shows perspective views of the $[Fe(Him)_2(salacen)]^+$ cation, with the atom numbering scheme. Table 3 lists relevant bond distances and angles with their estimated standard deviations in parentheses.

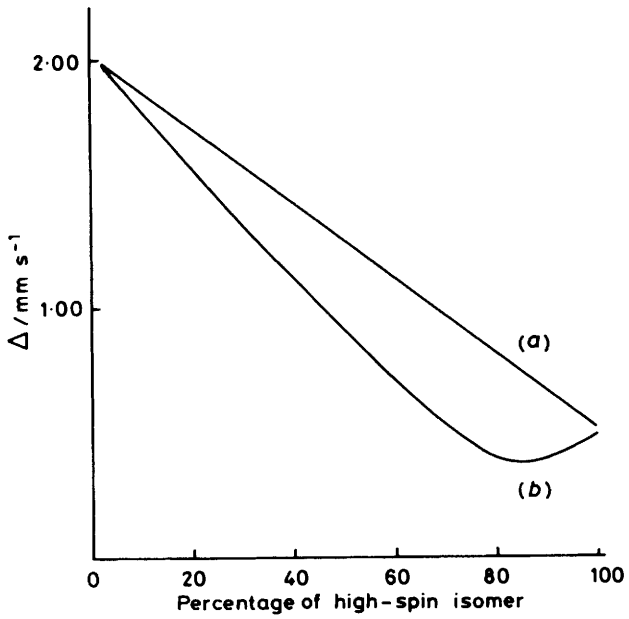

Figure 5. The variation of quadrupole splitting with the fraction of high-spin isomer in the limit of fast spin interconversion using the following parameters: $\tau_l = 1 \times 10^{-8}$ s, $\Delta_l = -2.00$ mm s^{-1}; (*a*) $\Delta_h = -0.50$, (*b*) $\Delta_h = +0.50$ mm s^{-1}

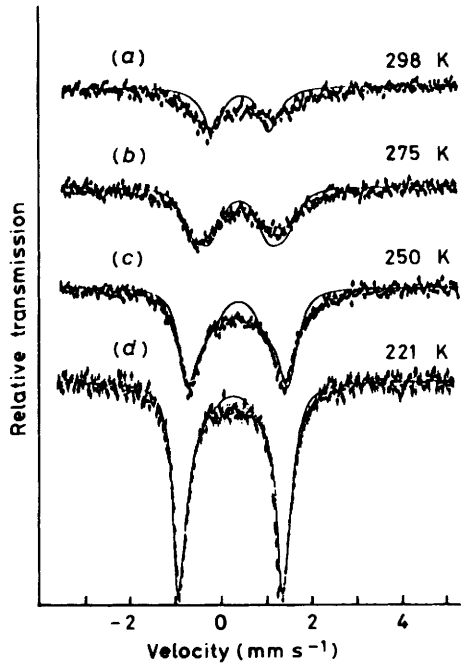

Figure 6. Representative attempt to obtain a best fit between the Mössbauer spectra for $[Fe(mim)_2(salacen)]PF_6$ and model (I). The full curves are calculated by using the following parameters: (*a*) $p_h = 75$, $\tau = 0.15$; (*b*) $p_h = 52$, $\tau = 0.23$; (*c*) $p_h = 33$, $\tau = 0.30$; (*d*) $p_h = 16\%$, $\tau = 0.32$ μs

The iron(III) atom is surrounded pseudo octahedrally by N_2O_2 donors of the unsymmetrical quadridentate salacen ligand in a plane and by two nitrogens of two imidazoles occupying the axial positions. The basal plane defined by Fe,

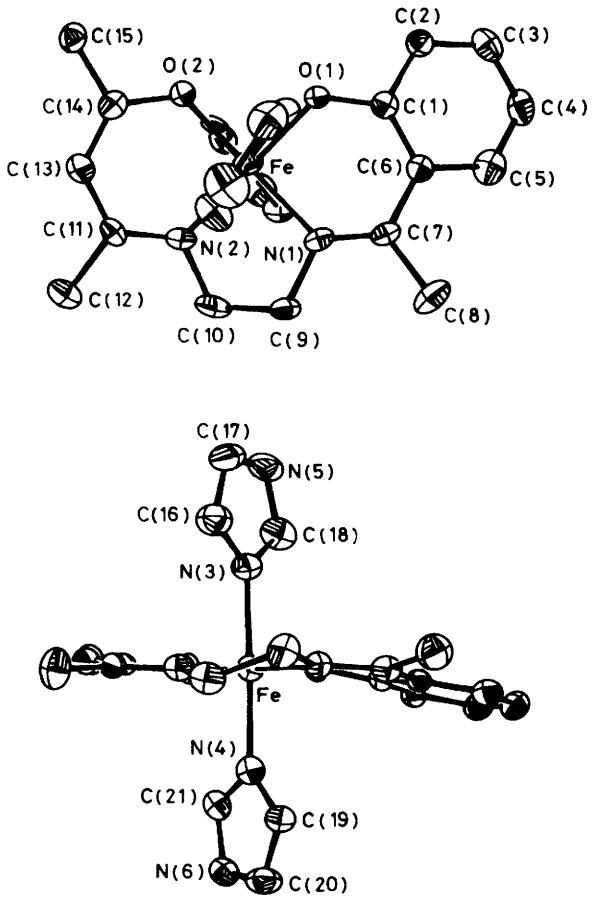

Figure 7. ORTEP drawings of $[Fe(Him)_2(salacen)]PF_6$ with the atom numbering scheme

O(1), O(2), N(1), and N(2) atoms is planar within the maximum deviation of 0.02 Å. The bond distance Fe–O(1) associated with the salicylaldehyde residue is shorter than Fe–O(2) associated with the acetylacetone residue, while Fe–N(1) is longer than Fe–N(2). The bonds to the imidazole nitrogens [Fe–N(3) 2.006(7), Fe–N(4) 2.027(7) Å] are longer than those to O(1), O(2), N(1), and N(2) atoms of the basal plane. Two imidazole rings (A and B) are not coplanar; the dihedral angle between them is 110.1°. The imidazole ring A lies approximately on O(1)–Fe–N(2), while the ring B lies on O(2)–Fe–N(1). The saturated five-membered chelate ring adopts a stable gauche conformation, where the atoms C(9) and C(10) deviate by 0.24 and −0.24 Å from the plane defined by Fe, N(1), and N(2). The six-membered chelate ring comprising the Fe atom and the acetylacetone residue is planar (maximum deviation of component atoms 0.04 Å).

It is known that iron–ligand distances for iron(III) complexes with N_4O_2 donors of sexidentate Schiff-base ligands are affected by the spin state of iron(III).[13] The magnetic moment for the present complex is 2.83 B.M. at the temperature which the *X*-ray diffraction study was performed. By assuming a simple additive property for the magnetic susceptibility, the low-spin population is estimated to be 83%. The average iron–ligand distance for the present complex (1.945 Å) is close to those of the low-spin complexes,[13] being consistent with the magnetic properties. We were not able to determine the molecular structure of $[Fe(mim)_2(salacen)]PF_6$.

Table 2. Atomic parameters for $[Fe(Him)_2(salacen)]PF_6$

Atom[a]	x	y	z	Atom[a]	x	y	z
Fe	3 095(1)	3 129(1)	781(1)	C(8)	1 912(12)	74(8)	−1 382(12)
O(1)	4 752(5)	2 849(4)	631(6)	C(9)	846(9)	1 627(8)	−107(11)
O(2)	3 975(5)	4 380(4)	1 857(6)	C(10)	357(9)	2 645(8)	56(12)
N(1)	2 225(7)	1 829(5)	−235(8)	C(11)	1 145(9)	4 175(7)	1 662(10)
N(2)	1 408(7)	3 395(6)	954(8)	C(12)	−254(10)	4 304(9)	1 651(12)
N(3)	2 868(6)	3 906(5)	−1 101(8)	C(13)	2 099(9)	4 926(7)	2 440(10)
N(4)	3 370(7)	2 386(6)	2 717(8)	C(14)	3 428(9)	5 032(7)	2 524(10)
N(5)	2 977(8)	5 207(6)	−2 569(9)	C(15)	4 356(10)	5 894(8)	3 374(11)
N(6)	4 403(9)	1 670(7)	4 686(9)	C(16)	2 140(9)	3 584(7)	−2 491(10)
C(1)	4 996(9)	2 129(7)	−252(10)	C(17)	2 238(10)	4 394(8)	−3 381(11)
C(2)	6 282(9)	2 255(7)	−459(10)	C(18)	3 342(8)	4 899(7)	−1 193(11)
C(3)	6 655(10)	1 557(9)	−1 340(11)	C(19)	2 483(11)	2 086(9)	3 536(11)
C(4)	5 749(10)	723(8)	−2 015(10)	C(20)	3 133(13)	1 647(10)	4 754(13)
C(5)	4 494(10)	572(8)	−1 848(10)	C(21)	4 493(9)	2 102(8)	3 395(11)
C(6)	4 060(9)	1 282(7)	−992(9)	P	−1 484(3)	2 107(2)	4 877(3)
C(7)	2 715(8)	1 134(7)	−852(9)				

Atom[b]	x	y	x	O.f.[c]	Atom[b]	x	y	z	O.f.[c]
F(1)	−68(2)	188(2)	384(3)	0.4	F(7)	−72(1)	178(1)	642(1)	0.6
F(2)	−217(1)	220(1)	318(1)	0.7	F(8)	−250(2)	257(2)	560(3)	0.4
F(3)	−24(1)	293(1)	478(2)	0.6	F(9)	−238(2)	303(1)	461(2)	0.5
F(4)	−243(1)	107(1)	464(3)	0.6	F(10)	−277(2)	152(2)	528(2)	0.4
F(5)	−125(3)	94(2)	478(3)	0.3	F(11)	−74(2)	332(1)	516(2)	0.5
F(6)	−113(2)	233(1)	658(2)	0.5	F(12)	−45(2)	138(2)	476(2)	0.4

[a] Parameters are multiplied by 10^4. [b] Parameters are multiplied by 10^3. [c] Occupancy factor.

Table 3. Bond distances (Å) and angles (°) for $[Fe(Him)_2(salacen)]PF_6$

Fe–O(1)	1.879(6)	C(3)–C(4)	1.389(13)	N(2)–C(10)	1.475(11)	N(6)–C(20)	1.365(17)
Fe–O(2)	1.911(5)	C(4)–C(5)	1.373(15)	N(2)–C(11)	1.230(12)	N(6)–C(21)	1.353(13)
Fe–N(1)	1.936(6)	C(5)–C(6)	1.407(14)	C(11)–C(12)	1.515(14)	N(4)–C(21)	1.305(11)
Fe–N(2)	1.912(7)	C(1)–C(6)	1.435(11)	C(11)–C(13)	1.378(11)	N(3)–C(16)	1.387(10)
Fe–N(3)	2.006(7)	C(6)–C(7)	1.459(13)	C(13)–C(14)	1.387(14)	C(16)–C(17)	1.339(14)
Fe–N(4)	2.027(7)	C(7)–C(8)	1.527(12)	O(2)–C(14)	1.315(12)	N(5)–C(17)	1.342(12)
O(1)–C(1)	1.332(11)	N(1)–C(7)	1.289(12)	C(14)–C(15)	1.481(12)	N(5)–C(18)	1.333(12)
C(1)–C(2)	1.419((4)	N(1)–C(9)	1.493(12)	N(4)–C(19)	1.377(14)	N(3)–C(18)	1.317(11)
C(2)–C(3)	1.377(15)	C(9)–C(10)	1.480(15)	C(19)–C(20)	1.346(15)		
P–F(1)	1.50(2)	P–F(4)	1.55(1)	P–F(7)	1.57(1)	P–F(10)	1.61(2)
P–F(2)	1.61(1)	P–F(5)	1.55(3)	P–F(8)	1.58(3)	P–F(11)	1.64(2)
P–F(3)	1.60(1)	P–F(6)	1.57(2)	P–F(9)	1.59(2)	P–F(12)	1.54(2)
O(1)–Fe–O(2)	86.4(2)	C(2)–C(3)–C(4)	118.7(10)	C(11)–C(13)–C(14)	127.8(9)		
O(1)–Fe–N(1)	93.2(2)	C(3)–C(4)–C(5)	122.6(10)	Fe–O(2)–C(14)	125.3(5)		
O(1)–Fe–N(2)	179.0(2)	C(4)–C(5)–C(6)	120.6(8)	O(2)–C(14)–C(13)	123.2(7)		
N(1)–Fe–N(2)	86.3(3)	C(1)–C(6)–C(5)	117.3(8)	O(2)–C(14)–C(15)	114.0(8)		
O(2)–Fe–N(2)	94.0(2)	C(1)–C(6)–C(7)	122.3(8)	C(13)–C(14)–C(15)	122.8(9)		
O(2)–Fe–N(1)	177.6(2)	C(5)–C(6)–C(7)	120.4(7)	Fe–N(3)–C(16)	129.6(5)		
N(3)–Fe–O(1)	90.0(2)	N(1)–C(7)–C(6)	122.7(7)	Fe–N(3)–C(18)	123.7(5)		
N(3)–Fe–O(2)	90.8(2)	N(1)–C(7)–C(8)	120.2(8)	C(16)–N(3)–C(18)	106.5(7)		
N(3)–Fe–N(1)	91.5(2)	C(6)–C(7)–C(8)	117.0(8)	N(3)–C(16)–C(17)	107.7(7)		
N(3)–Fe–N(2)	90.9(3)	Fe–N(1)–C(7)	128.5(6)	C(16)–C(17)–N(5)	107.6(8)		
N(3)–Fe–N(4)	178.1(2)	Fe–N(1)–C(9)	111.0(5)	C(17)–N(5)–C(18)	108.4(7)		
N(4)–Fe–O(1)	89.4(2)	C(7)–N(1)–C(9)	120.3(7)	N(3)–C(18)–N(5)	109.7(7)		
N(4)–Fe–O(2)	87.3(2)	N(1)–C(9)–C(10)	109.4(7)	Fe–N(4)–C(19)	129.1(6)		
N(4)–Fe–N(1)	90.4(2)	C(9)–C(10)–N(2)	110.1(7)	Fe–N(4)–C(21)	122.8(6)		
N(4)–Fe–N(2)	89.7(3)	Fe–N(2)–C(10)	112.0(6)	C(19)–N(4)–C(21)	108.2(8)		
Fe–O(1)–C(1)	126.2(4)	Fe–N(2)–C(11)	126.7(5)	N(4)–C(19)–C(20)	107.1(10)		
O(1)–C(1)–C(2)	115.2(7)	C(10)–N(2)–C(11)	121.1(7)	C(19)–C(20)–N(6)	108.1(11)		
O(1)–C(1)–C(6)	124.8(8)	N(2)–C(11)–C(13)	122.7(9)	C(20)–N(6)–C(21)	106.8(8)		
C(2)–C(1)–C(6)	120.0(8)	N(2)–C(11)–C(12)	120.6(7)	N(4)–C(21)–N(6)	109.8(9)		
C(1)–C(2)–C(3)	120.7(8)	C(12)–C(11)–C(13)	116.8(9)				

Spin Equilibrium in Solution.—The complexes $[Fe(Him)_2(salacen)]PF_6$ and $[Fe(mim)_2(salacen)]PF_6$ were reversibly thermochromic in solution, changing colour from purple at room temperature to green at *ca.* 200 K (solid CO_2/solvent) in various organic solvents although the former complex is low-spin in the solid state. The electronic spectra for $[Fe(Him)_2$-

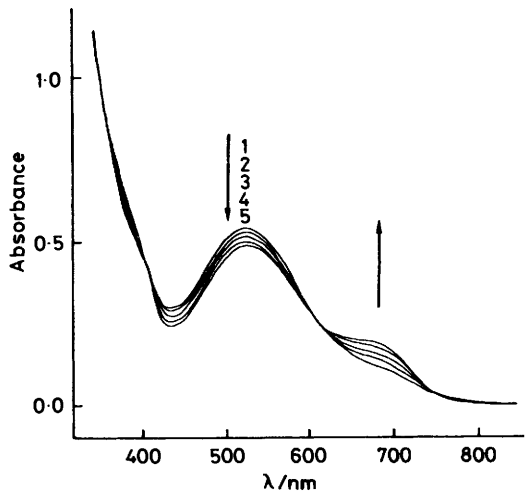

Figure 8. Temperature dependences of the electronic spectra of $[Fe(Him)_2(salacen)]PF_6$ in dichloromethane solution: (1) 289, (2) 268, (3) 258, (4) 248, (5) 243 K

(salacen)]PF_6 in dichloromethane solution were recorded at various temperatures. Absorption spectra are shown in Figure 8; that at 289 K has a strong band at 525 nm and a shoulder at 680 nm. On cooling down to 243 K, the absorption at 525 nm decreases in intensity and that at 680 nm increases. The absorptions at 525 and 680 nm are due to high-and low-spin species, respectively. The temperature dependence of the spectra should be accompanied by spin-equilibrium behaviour. The differences in the magnetic behaviour of the cation $[Fe(Him)_2(salacen)]^+$ in the solid and in solution show that in the solid the crystal packing, and in solution the chemical form of a cation and its interaction with the solvent play important roles. The difference in the behaviour of the spin conversion in the solid and in solution has also been observed for other spin-crossover systems.[9,31] The difference in crystal packing between Him and mim may bring about the difference in the spin-crossover behaviour between $[Fe(mim)_2(salacen)]PF_6$ and $[Fe(Him)_2(salacen)]PF_6$ because the spin-crossover phenomena in solution take place through an intramolecular mechanism.

Acknowledgements

We thank the Institute for Molecular Science for use of the *X*-ray diffractometer (the Instrument Centre) and the Computer (the Computer Centre). This work was partially supported by a grant-in-aid for scientific research from the Ministry of Education, Science and Culture, Japan.

References

1 L. Cambi, L. Szego, and A. Cagnasso, *Atti Accad. Naz. Lincei Cl. Sci. Fis., Mat. Nat. Rend.*, 1932, **15**, 266.
2 A. H. Ewald, R. L. Martin, I. G. Ross, and A. H. White, *Proc. R. Soc. London, Ser. A*, 1964, **280**, 235.
3 Y. Maeda, Y. Takashima, and Y. Nishida, *Bull. Chem. Soc. Jpn.*, 1976, **49**, 2427.
4 Y. Maeda, S. Shite, Y. Takashima, and Y. Nishida, *Bull. Chem. Soc. Jpn.*, 1977, **50**, 2902.
5 P. Gütlich, *Struct. Bonding (Berlin)*, 1981, **44**, 83.
6 E. König, G. Ritter, W. Irler, and H. A. Goodwin, *J. Am. Chem. Soc.*, 1980, **102**, 4681.
7 S. Kremer, W. Henke, and D. Reinen, *Inorg. Chem.*, 1982, **21**, 3013.
8 H. Ohshio, Y. Maeda, and Y. Takashima, *Inorg. Chem.*, 1983, **22**, 2684.
9 Y. Maeda, N. Tsutsumi, and Y. Takashima, *Inorg. Chem.*, 1984, **23**, 2440; *Chem. Phys. Lett.*, 1982, **88**, 248.
10 W. D. Federer and D. N. Hendrickson, *Inorg. Chem.*, 1984, **23**, 3861.
11 M. Cox, J. Darken, B. W. Fitzsimmons, A. W. Smith, L. F. Larkorthy, and K. A. Rogers, *J. Chem. Soc., Dalton Trans.*, 1972, 1192.
12 M. Sorai and S. Seki, *J. Phys. Chem. Solids*, 1974, **35**, 555.
13 E. Sinn, G. Sim, E. V. Dose, M. F. Tweedle, and L. J. Wilson, *J. Am. Chem. Soc.*, 1978, **100**, 3375.
14 T. Ito, M. Sugimoto, H. Ito, K. Toriumi, H. Nakayama, W. Mori, and M. Sekizaki, *Chem. Lett.*, 1983, 121.
15 N. Matsumoto, S. Ohta, C. Yoshimura, S. Kohata, H. Okawa, Y. Maeda, and A. Ohyoshi, *J. Chem. Soc., Dalton Trans.*, 1985, 2575.
16 B. F. Hoskins and C. D. Pannan, *Inorg. Nucl. Chem. Lett.*, 1975, **11**, 409.
17 N. Matsumoto, M. Asakawa, H. Nogami, and A. Ohyoshi, *Inorg. Chim. Acta*, 1985, **96**, 87; N. Matsumoto, M. Asakawa, H. Nogami, M. Higuchi, and A. Ohyoshi, *J. Chem. Soc., Dalton Trans.*, 1985, 101.
18 T. Sakurai, and K. Kobayashi, *Rikagaku Kenkyusho Hokoku*, 1979, **55**, 69; S. Kawano, *Rep. Comput. Cent. Kyushu Univ.*, 1980, **13**, 39.
19 'International Tables for *X*-Ray Crystallography,' Kynoch Press, Birmingham, 1974, vol. 4.
20 R. F. Stewart, E. R. Davidson, and W. T. Simpson, *J. Chem. Phys.*, 1965, **42**, 3175.
21 P. W. Anderson and P. R. Weiss, *Rev. Mod. Phys.*, 1953, **25**, 269.
22 R. Kubo, *J. Phys. Soc. Jpn.*, 1954, **9**, 935.
23 R. Kubo and K. Tomita, *J. Phys. Soc. Jpn.*, 1954, **9**, 888.
24 R. A. Sack, *Mol. Phys.*, 1958, **1**, 163.
25 M. Blume and J. A. Tjon, *Phys. Rev.*, 1968, **165**. 446.
26 J. A. Tjon and M. Blume, *Phys. Rev.*, 1968, **165**, 456.
27 A. Abragam, 'The Principles of Nuclear Magnetism,' Oxford University Press, London, 1961.
28 H. H. Wickman, 'Mössbauer Effect Methodology,' ed. I. J. Gruverman, Plenum Press, New York, 1966, p. 39.
29 E. Buhks, G. Navon, M. Bixon, and J. Jortner, *J. Am. Chem. Soc.*, 1980, **102**, 2918.
30 N. Sutin, *Acc. Chem. Res.*, 1982, **15**, 275.
31 E. V. Dose, M. A. Hoselton, N. Sutin, M. F. Tweedle, and L. J. Wilson, *J. Am. Chem. Soc.*, 1978, **100**, 1141.

Received 15*th July* 1985; *Paper* 5/1186